Reduction of Nonlinear Models for Control Applications

A. Da Ronch, * N. D. Tantaroudas † and K. J. Badcock ‡
University of Liverpool, Liverpool, England L69 3BX, United Kingdom

A systematic approach to the model reduction of high-fidelity fluid-structure-flight models and the subsequent flight control design for very flexible aircraft is considered. The test case is for an unmanned aerial vehicle. The full order model involves the geometrically-exact nonlinear beam equations coupled with a linear aerodynamic model. A nonlinear reduced order model is derived to reduce the computational cost and dimension of the full order nonlinear system while retaining the ability to predict nonlinear effects. The approach uses information on the eigenspectrum of the coupled system Jacobian matrix and projects the system through a series expansion onto a small basis of eigenvectors representative of the full order dynamics. The small dimension model is then used to design control laws for applications sush as load alleviation. Results are presented for an aerofoil section and an unmanned aerial vehicle model to illustrate the approach.

Nomenclature

$\boldsymbol{A}$	= Jacobian matrix of $\boldsymbol{R}$ with respect to $\boldsymbol{w}$
$\boldsymbol{B}$, $\boldsymbol{C}$	= second and third Jacobian operators
b	= semichord
t	= physical time
$\boldsymbol{R}$	= residual vector
U	= freestream velocity
U_L	= linear flutter speed
U_L^*	= reduced velocity, $U/b\,\omega_\alpha$
$\boldsymbol{w}$	= vector of unknowns
W_0	= intensity of gust vertical velocity

Greek

α	= angle of attack
λ_i	= i-th eigenvalue of $\boldsymbol{A}$
τ	= nondimensional time, $t\,U/b$
ω_α	= uncoupled pitching mode natural frequency about elastic axis, $\sqrt{K_\alpha/I_\alpha}$
$\boldsymbol{\phi}_i$, $\boldsymbol{\psi}_i$	= i-th right and left eigenvectors of $\boldsymbol{A}$
ξ	= nondimensional displacement in plunge, h/b

Symbol

$\dot{(\,)}$	= differentiation with respect to t, $d(\,)/dt$
$(\,)'$	= differentiation with respect to τ, $d(\,)/d\tau$
$\bar{(\,)}$	= complex conjugation

*Research Associate, School of Engineering; A.Da-Ronch@liverpool.ac.uk. Member AIAA (Corresponding Author).
†Ph.D. Student, School of Engineering.
‡Professor, School of Engineering. Senior Member AIAA.

I. Introduction

The work detailed in this paper is part of the development of a systematic approach to flight control system (FCS) design for very flexible or very large aircraft. Examples of vehicles in this class are those considered for low-environmental impact air transport and for long-endurance unmanned operations. Improved aircraft performance is generally achieved through lightweight solutions with high aspect ratio wings for maximum aerodynamic efficiency. The combination of low structural weight fraction and high aerodynamic efficiency yields inherently flexible wings with a nonlinear structural and flight dynamics behaviour. The traditional separation of aeroelasticity and flight dynamics is therefore not appropriate for flight control when low structural frequencies, which are often associated with large amplitude motions, are present. The mishap of NASA's Helios aircraft demonstrated that (linear) traditional design methods are no longer adequate for the analysis of the next-generation aircraft.[1] Modelling and design methods based on a fully coupled system are therefore necessary.[2]

The use of high-fidelity fluid-structure-flight models results in large-order systems which are incompatible with control design as the bulk of control theory was developed for systems of relatively low order. This introduces the question of how to reduce the dimension of the large-order nonlinear system while retaining the ability to predict nonlinear effects. Traditional model reduction methods assume linearity or, at most, weak nonlinearities.[3] There are two approaches to model reduction. System identification methods take the response of the system to known inputs, and use this information to build a low-order model.[4,5] The disadvantages of these methods are the lack of a general robust parametrization of the model and the inability to predict any physics that is not included in the training data. However, these methods have met with success in computational flight dynamics[6,7] and aeroelasticity.[8] The second approach is to manipulate the full-order nonlinear residual to reduce the cost of calculations. The advantage in doing this is that the predictive capability of the full-order model (FOM) is retained. The disadvantage is the added technical complication of manipulating the system. An example is the harmonic balance method, which has been exploited for dynamic derivative predictions avoiding costly time-accurate computational fluid dynamics (CFD) runs.[9,10] The second approach is used in this work. The focus herein is on the development of nonlinear ROMs for control design, derived from large-order CFD-based models and nonlinear beam models, and control design is demonstrated for gust load alleviation for an aircraft test problem.

One approach presented in Refs.[11,12] is to project the full-order model onto the critical mode and expand the residual in Taylor series, retaining quadratic and cubic terms. The method has been successfully applied to various testcases, including the LCO prediction dominated by the motion of a shock wave[11] and a prototype flight dynamics instability of a delta wing.[12] The approach to model reduction has been generalized in Ref.[13] by using multiple coupled system eigenmodes for model projection and introducing control deflection and gust interaction effects into the formulation.

A large body of work has been done on control of a two-dimensional aeroelastic system with structural nonlinearities as reported, for example, in Refs.[14,15] A nonlinear feedback control law based on the state-dependent Riccati equation was presented in Ref.,[14] and Ref.[15] applied a partial feedback linearization to control LCO of a wind tunnel model. More recently, control design has been shown for stability augmentation and gust load alleviation in flexible aircraft .[16,17] A common approach was to fully account for the nonlinear structural behaviour while simple linear aerodynamic models based on two-dimensional theory and panel methods were used for the aerodynamics. Standard linear control design methods may also be inadequate for highly flexible aircraft because the dynamic behaviour is intrinsically nonlinear.

The objective of this paper is to apply a systematic approach to model reduction of a large-order fluid-structure-flight model and the subsequent flight control design of a very flexible aircraft. The paper expands on previous work,[13] where the model reduction was applied to different test cases with a range of nonlinearities in both fluid and structural models and it was shown that control problem is possible on the reduced models generated. This paper demonstrates the use of the model reduction for a full-scale flexible unmanned aerial vehicle (UAV) interacting with gust and using control surfaces for loads alleviation. The nonlinear large-order model is derived by coupling a linear aerodynamic model with a multi-body nonlinear beam code for unrestrained bodies.[2] A companion paper will present the challenges and approaches in simulating gust interaction with CFD.

The paper continues with an overview of the nonlinear coupled system of equations in § II. The model reduction is formulated in § III, followed by a description of the algorithm used in calculating the Jacobian operators and the approach to solve large-order eigenvalue problem. The use of reduced models for control is detailed in § IV. The paper then continues with results for two test cases, and conclusions are finally given

in § VII.

II. Full Order Model

The fully coupled nonlinear model for the description of the flight dynamics of a very flexible aircraft can be represented in a state-space form. Denote by $\boldsymbol{w}$ the n-dimensional state-space vector which is conveniently partitioned into fluid, structural and rigid body degrees of freedom

$$\boldsymbol{w} = \left[\boldsymbol{w}_f^T, \boldsymbol{w}_s^T, \boldsymbol{w}_r^T\right]^T \tag{1}$$

The state-space equations in the general vector form are

$$\frac{d\,\boldsymbol{w}}{dt} = \boldsymbol{R}\left(\boldsymbol{w}, \boldsymbol{u}_c, \boldsymbol{u}_d\right) \tag{2}$$

where $\boldsymbol{R}$ is the (nonlinear) residual, $\boldsymbol{u}_c$ is the input vector, and $\boldsymbol{u}_d$ is the exogenous vector for the description of some form of disturbance acting on the system. The homogeneous system has an equilibrium point, $\boldsymbol{w}_0$, for given constant $\boldsymbol{u}_{c\,0}$ and $\boldsymbol{u}_{d\,0}$ corresponding to a constant solution in the state space and satisfying

$$\frac{d\,\boldsymbol{w}_0}{dt} = \boldsymbol{R}\left(\boldsymbol{w}_0, \boldsymbol{u}_{c\,0}, \boldsymbol{u}_{d\,0}\right) = \boldsymbol{0} \tag{3}$$

The residual form in Eq. (2) forms the basis for the model reduction described below. The system is often parametrized in terms of an independent parameter (freestream speed, air density, altitude, etc.) for stability analysis. The options for the residual evaluation are described in the next section.

II.A. Residual Definition

The formulation of the previous section is given in terms of the residual function $\boldsymbol{R}$. Several options are used in this paper to define the residual. The options are summarised in this section.

II.A.1. Linear Aerodynamic Model

The linear aerodynamic model used here is based on strip theory and the incompressible two–dimensional classical theory of Theodorsen. The total aerodynamic loads consist of contributions arising from the section motion, flap deflection and the penetration into a gusty field. The aerodynamic loads due to an arbitrary input time-history are obtained through convolution against a kernel function. For the influence of the aerofoil motion on the loads, the Wagner function is used. For the response to a sharp edged gust, the integration uses the Küssner function. Since the assumption is of linear aerodynamics, the effects of the two influences on the aerodynamic forces and moments are added together to find the variation of the forces and moments in time for a given motion and gust. For a practical evaluation of the integral, an exponential approximation is used for the Wagner and Küssner functions. The aerodynamic state vector for this model has dimension 8, and the formulation in terms of a residual function follows that given in Ref.[18]

Two families of atmospheric gust are used in this paper. The discrete model for the "1 minus cosine" gust is formulated as

$$W_g\left(\tau\right) = \frac{W_0}{2}\cos\left(\frac{2\,\pi}{H_g}\left(\tau - \tau_0\right)\right) \qquad \text{for } \tau_0 \le \tau \le \tau_0 + H_g \tag{4}$$

where W_0 is the gust intensity normalized by the freestream speed and H_g is the gust length. For a continuous model of atmospheric turbulence, the Von Kármán spectrum is used because it provides a good approximation to real atmospheric spectra which tend to fall off as $f^{-5/3}$ in the frequency range of interest to aircraft response. Because the transfer function of the Von Kármán model is irrational, the rational approximation documented in Ref.[19] is used in this paper.

II.A.2. Two Degree-of-Freedom Model

A typical aerofoil section has two degrees of freedom that define the motion about a reference elastic axis (*e.a.*). The plunge deflection is denoted by h, positive downward, and α is the angle of attack about the

elastic axis, positive with nose up. The aerofoil is equipped with a massless trailing-edge flap with hinge at a distance $c\,b$ from the midchord. The flap deflection, δ, is defined relative to the undeflected position. The motion is restrained by two springs, K_ξ and K_α, and is assumed to have a horizontal equilibrium position at $h = \alpha = \delta = 0$. The system also contains structural damping in both degrees of freedom.

The equations of motion in dimensional form with nonlinear restoring forces in pitch and plunge can be derived, for example, using the Lagrange equations[20]

$$m\,\ddot{h} + S_\alpha\,\ddot{\alpha} + C_\xi\,\dot{h} + K_\xi\left(h + \beta_\xi\,h^3 + \beta_{\xi_5}\,h^5\right) = -L \tag{5}$$

$$S_\alpha\,\ddot{h} + I_\alpha\,\ddot{\alpha} + C_\alpha\,\dot{\alpha} + K_\alpha\left(\alpha + \beta_\alpha\,\alpha^3 + \beta_{\alpha_5}\,\alpha^5\right) = M \tag{6}$$

with the structural nonlinearity approximated in a polynomial form.[21] The lift, L, is defined positive upward according to the usual sign convention in aerodynamics. The plunge displacement, h, is positive downward, as it is conventionally done in aeroelasticity. In nondimensional form, the equations of motion become

$$\xi'' + x_\alpha\,\alpha'' + 2\,\zeta_\xi\,\frac{\bar{\omega}}{U^*}\,\xi' + \left(\frac{\bar{\omega}}{U^*}\right)^2\left(\xi + \beta_\xi\,\xi^3 + \beta_{\xi_5}\,\xi^5\right) = -\frac{1}{\pi\,\mu}\,C_L\,(\tau) \tag{7}$$

$$\frac{x_\alpha}{r_a^2}\,\xi'' + \alpha'' + 2\,\zeta_\alpha\,\frac{1}{U^*}\,\alpha' + \left(\frac{1}{U^*}\right)^2\left(\alpha + \beta_\alpha\,\alpha^3 + \beta_{\alpha_5}\,\alpha^5\right) = \frac{2}{\pi\,\mu\,r_a^2}\,C_m\,(\tau) \tag{8}$$

where nondimensional parameters are defined in the nomenclature. Differentiation with respect to t, indicated by $\dot{(\,)}$, is replaced by a differentiation with respect to τ, $\dot{(\,)} = U/b\,(\,)'$. These equations are rewritten to define a residual contribution.

II.A.3. Nonlinear Beam Model

For the structural model, the geometrically-exact nonlinear beam equations are used.[22] Results are obtained using two-noded displacement-based elements. In a displacement-based formulation, nonlinearities arising from large deformations are cubic terms, as opposed to an intrinsic description where they appear up to second order. The finite element beam code used in this study has been tested extensively, and more details can be found, for example, in Ref.[2] The nonlinear beam code was coupled with strip aerodynamics. At each beam node, the coupled system includes 6 degrees of freedom for the structural model and 8 for the aerodynamic model. For each aerofoil section, aerodynamic forces are treated as follower forces that depend on the local instantaneous angle of attack of the wing aerofoil.

III. Nonlinear Model Reduction

Denote $\Delta\boldsymbol{w} = \boldsymbol{w} - \boldsymbol{w}_0$ the increment in the state-space vector with respect to an equilibrium solution. The large-order nonlinear residual formulated in Eq. (2) is expanded in a Taylor series around the equilibrium point

$$\boldsymbol{R}\,(\boldsymbol{w}) \approx \boldsymbol{A}\,\Delta\boldsymbol{w} + \frac{\partial\,\boldsymbol{R}}{\partial\,\boldsymbol{u}_c}\,\Delta\boldsymbol{u}_c + \frac{\partial\,\boldsymbol{R}}{\partial\,\boldsymbol{u}_d}\,\Delta\boldsymbol{u}_d + \frac{1}{2}\,\boldsymbol{B}\,(\Delta\boldsymbol{w},\,\Delta\boldsymbol{w}) + \frac{1}{6}\,\boldsymbol{C}\,(\Delta\boldsymbol{w},\,\Delta\boldsymbol{w},\,\Delta\boldsymbol{w}) + \mathcal{O}\left(|\Delta\boldsymbol{w}|^4\right) \tag{9}$$

retaining terms up to third order in the perturbation variable. The Jacobian matrix of the system is denoted as $\boldsymbol{A}$ and the vectors $\boldsymbol{B}$ and $\boldsymbol{C}$ indicate, respectively, the second and third order Jacobian operators. The elements are calculated as

$$\begin{aligned} A_{ij} &= \frac{\partial\,R_i\,(\boldsymbol{w}_0)}{\partial\,w_j} \\ B_i\,(\boldsymbol{x},\,\boldsymbol{y}) &= \sum_{j,\,k}\frac{\partial^2\,R_i\,(\boldsymbol{w}_0)}{\partial\,w_j\,\partial\,w_k}\,x_j\,y_k \\ C_i\,(\boldsymbol{x},\,\boldsymbol{y},\,\boldsymbol{z}) &= \sum_{j,\,k,\,l}\frac{\partial^3\,R_i\,(\boldsymbol{w}_0)}{\partial\,w_j\,\partial\,w_k\,\partial\,w_l}\,x_j\,y_k\,z_l \end{aligned} \tag{10}$$

The full-order system is projected onto a basis formed by a small number (denoted by m) of eigenvectors of the Jacobian matrix evaluated at the equilibrium position. A rational choice would be to retain only the

slow modes since they are likely to dominate the system dynamics in the absence of instability. The right and left eigenvalues and eigenvectors are complex in general. The set of right eigenvectors $\boldsymbol{\phi}_i$ is obtained by solving

$$\boldsymbol{A}\,\boldsymbol{\phi}_i \;=\; \lambda_i\,\boldsymbol{\phi}_i \quad \text{for } i \;=\; 1,\ldots,n \tag{11}$$

The set of left eigenvectors, $\boldsymbol{\psi}_i$, are obtained by solving the adjoint eigenvalue problem

$$\boldsymbol{A}^T\,\boldsymbol{\psi}_i \;=\; \lambda_i\,\boldsymbol{\psi}_i \quad \text{for } i \;=\; 1,\ldots,n \tag{12}$$

If all the eigenvalues are distinct, the right and left eigenvectors corresponding to different eigenvalues are biorthogonal. It is then convenient to normalize the eigenvectors so as to satisfy the biorthonormality conditions, expressed by

$$<\boldsymbol{\phi}_i,\,\boldsymbol{\phi}_i>\;=\;1, \quad <\boldsymbol{\psi}_j,\,\boldsymbol{\phi}_i>\;=\;\delta_{ij}, \quad <\boldsymbol{\psi}_j,\,\bar{\boldsymbol{\phi}}_i>\;=\;0 \quad \text{for } i,j \;=\; 1,\ldots,m \tag{13}$$

and resulting in

$$<\boldsymbol{\psi}_j,\,\boldsymbol{A}\,\boldsymbol{\phi}_i>\;=\;\lambda_i\,\delta_{ij}, \quad <\boldsymbol{\psi}_j,\,\boldsymbol{A}\,\bar{\boldsymbol{\phi}}_i>\;=\;0 \quad \text{for } i,j \;=\; 1,\ldots,m \tag{14}$$

where δ_{ij} is the Kronecker delta. Note that the Hermitian inner product is defined as $<\boldsymbol{x},\boldsymbol{y}>\;=\bar{\boldsymbol{x}}^T\,\boldsymbol{y}$, with the overbar denoting complex conjugation. The $(n\times m)$ right and left modal matrices, respectively, $\boldsymbol{\Phi}$ and $\boldsymbol{\Psi}$, are formed as

$$\boldsymbol{\Phi} \;=\; [\boldsymbol{\phi}_1,\,\ldots,\,\boldsymbol{\phi}_m]\,, \quad \boldsymbol{\Psi} \;=\; [\boldsymbol{\psi}_1,\,\ldots,\,\boldsymbol{\psi}_m] \tag{15}$$

The full order model is projected onto a small basis of m representative eigenvectors using a transformation of coordinates

$$\Delta\boldsymbol{w} \;=\; \boldsymbol{\Phi}\,\boldsymbol{z} \;+\; \bar{\boldsymbol{\Phi}}\,\bar{\boldsymbol{z}} \tag{16}$$

where $\boldsymbol{z}\in\mathbb{C}^m$ is the state-space vector governing the dynamics of the reduced-order nonlinear system.

When nonlinear terms in the Taylor series expansion of the large-order nonlinear residual are neglected, a linear reduced model can be derived. Substituting the transformation of coordinates in Eq. (16) into Eq. (9) and premultiplying each term by the conjugate transpose of the left modal matrix yields

$$\bar{\boldsymbol{\psi}}_j^T\,\left(\boldsymbol{\phi}_i\,z_i' \;+\; \bar{\boldsymbol{\phi}}_i\,\bar{z}_i'\right) \;=\; \bar{\boldsymbol{\psi}}_j^T\,\left(\boldsymbol{A}\,\boldsymbol{\phi}_i\,z_i \;+\; \boldsymbol{A}\,\bar{\boldsymbol{\phi}}_i\,\bar{z}_i \;+\; \frac{\partial\,\boldsymbol{R}}{\partial\,\boldsymbol{u}_c}\,\Delta\boldsymbol{u}_c \;+\; \frac{\partial\,\boldsymbol{R}}{\partial\,\boldsymbol{u}_d}\,\Delta\boldsymbol{u}_d\right) \qquad \text{for } i,j \;=\; 1,\ldots,m \tag{17}$$

If the eigenvalues are distinct, which is not always the case, the properties in Eqs. (13) and (14) yield a linear ROM

$$z_i' \;=\; \lambda_i\,z_i \;+\; \bar{\boldsymbol{\psi}}_i^T\,\left(\frac{\partial\,\boldsymbol{R}}{\partial\,\boldsymbol{u}_c}\,\Delta\boldsymbol{u}_c \;+\; \frac{\partial\,\boldsymbol{R}}{\partial\,\boldsymbol{u}_d}\,\Delta\boldsymbol{u}_d\right) \qquad \text{for } i \;=\; 1,\ldots,m \tag{18}$$

The set of equations in Eq. (18) consists of m uncoupled ordinary differential equations (ODEs). The terms of the reduced model are calculated once and for all after the eigenvalues, eigenvectors, and equilibrium are known. For large-order coupled systems, as those arising using CFD, the solution of the eigenvalue problem is a challenging task and the use of standard routines is impractical. The Schur complement eigenvalue solver from the University of Liverpool was developed for this specific problem and was applied to realistically sized aeroelastic models.[23]

Manipulation of the higher-order terms in Eq. (9) yield the formulation of a nonlinear ROM. In addition to the linear terms in Eq. (17), the two contributions from the second and third Jacobian operators are

$$\bar{\boldsymbol{\psi}}_j^T\,\left(\frac{1}{2}\,B_i\,(\Delta\boldsymbol{w},\,\Delta\boldsymbol{w}) \;+\; \frac{1}{6}\,C_i\,(\Delta\boldsymbol{w},\,\Delta\boldsymbol{w},\,\Delta\boldsymbol{w})\right) \tag{19}$$

The terms $\boldsymbol{B}$ and $\boldsymbol{C}$ are, respectively, bilinear and trilinear functions in the argument variables. This property implies that, after substitution of the transformation of coordinates, the additional terms may be written as

$$\begin{aligned} B_i\,(\Delta\boldsymbol{w},\,\Delta\boldsymbol{w}) \;=\; \sum_{r\,=\,1}^{m}\,\sum_{s\,=\,1}^{m}\,\Big(&B_i\,(\boldsymbol{\phi}_r,\,\boldsymbol{\phi}_s)\;z_r\,z_s \;+\; B_i\,\left(\boldsymbol{\phi}_r,\,\bar{\boldsymbol{\phi}}_s\right)\;z_r\,\bar{z}_s \;+ \\ &B_i\,\left(\bar{\boldsymbol{\phi}}_r,\,\boldsymbol{\phi}_s\right)\;\bar{z}_r\,z_s \;+\; B_i\,\left(\bar{\boldsymbol{\phi}}_r,\,\bar{\boldsymbol{\phi}}_s\right)\;\bar{z}_r\,\bar{z}_s\Big) \end{aligned} \tag{20}$$

and

$$C_i\left(\Delta\boldsymbol{w},\,\Delta\boldsymbol{w},\,\Delta\boldsymbol{w}\right) = \sum_{r=1}^{m}\sum_{s=1}^{m}\sum_{t=1}^{m}\Big(C_i\left(\boldsymbol{\phi}_r,\,\boldsymbol{\phi}_s,\,\boldsymbol{\phi}_t\right)\,z_r\,z_s\,z_t + C_i\left(\boldsymbol{\phi}_r,\,\boldsymbol{\phi}_s,\,\bar{\boldsymbol{\phi}}_t\right)\,z_r\,z_s\,\bar{z}_t + C_i\left(\boldsymbol{\phi}_r,\,\bar{\boldsymbol{\phi}}_s,\,\boldsymbol{\phi}_t\right)\,z_r\,\bar{z}_s\,z_t + C_i\left(\boldsymbol{\phi}_r,\,\bar{\boldsymbol{\phi}}_s,\,\bar{\boldsymbol{\phi}}_t\right)\,z_r\,\bar{z}_s\,\bar{z}_t + C_i\left(\bar{\boldsymbol{\phi}}_r,\,\boldsymbol{\phi}_s,\,\boldsymbol{\phi}_t\right)\,\bar{z}_r\,z_s\,z_t + C_i\left(\bar{\boldsymbol{\phi}}_r,\,\boldsymbol{\phi}_s,\,\bar{\boldsymbol{\phi}}_t\right)\,\bar{z}_r\,z_s\,\bar{z}_t + C_i\left(\bar{\boldsymbol{\phi}}_r,\,\bar{\boldsymbol{\phi}}_s,\,\boldsymbol{\phi}_t\right)\,\bar{z}_r\,\bar{z}_s\,z_t + C_i\left(\bar{\boldsymbol{\phi}}_r,\,\bar{\boldsymbol{\phi}}_s,\,\bar{\boldsymbol{\phi}}_t\right)\,\bar{z}_r\,\bar{z}_s\,\bar{z}_t\Big) \tag{21}$$

The second and third order Jacobians consist, in general, of $4\,m^2$ and $8\,m^3$ contributions. However, it is possible to exploit the symmetry of the Jacobians with respect to the arguments [a], which reduces the total number of evaluations to $2\,m^2+m$ in the case of the bilinear function. Equation (20) can then be rearranged as

$$B_i\left(\Delta\boldsymbol{w},\,\Delta\boldsymbol{w}\right) = \sum_{r=1}^{m}\Big(B_i\left(\boldsymbol{\phi}_r,\,\boldsymbol{\phi}_r\right)\,z_r^2 + 2\,B_i\left(\boldsymbol{\phi}_r,\,\bar{\boldsymbol{\phi}}_r\right)\,z_r\,\bar{z}_r + B_i\left(\bar{\boldsymbol{\phi}}_r,\,\bar{\boldsymbol{\phi}}_r\right)\,\bar{z}_r^2 + 2\sum_{s=r+1}^{m}\Big(B_i\left(\boldsymbol{\phi}_r,\,\boldsymbol{\phi}_s\right)\,z_r\,z_s + B_i\left(\boldsymbol{\phi}_r,\,\bar{\boldsymbol{\phi}}_s\right)\,z_r\,\bar{z}_s + B_i\left(\bar{\boldsymbol{\phi}}_r,\,\boldsymbol{\phi}_s\right)\,\bar{z}_r\,z_s + B_i\left(\bar{\boldsymbol{\phi}}_r,\,\bar{\boldsymbol{\phi}}_s\right)\,\bar{z}_r\,\bar{z}_s\Big)\Big) \tag{22}$$

For the third order Jacobian term, the total number of evaluations may be reduced to $2/3\left(2\,m^3+3\,m^2+m\right)$. For conciseness, the corresponding formulation of $\boldsymbol{C}$ is omitted.

The high-order Jacobian terms required in the model reduction are represented by the bilinear and trilinear functionals formulated in Eq. (10). It is possible to calculate all the contributions without having to resort to complex arithmetic, or to calculating all the second and third order partial derivatives analytically.[11] Because it is only their action on vectors that is required, matrix-free products are used.

For the first order Jacobian-vector product and for the second and third Jacobian operators, the directional derivatives on any set of coinciding real vectors, $\boldsymbol{x}\in\mathbb{R}^n$, can be approximated using finite differences

$$\boldsymbol{A}\,\boldsymbol{x} = \frac{\boldsymbol{R}_1-\boldsymbol{R}_{-1}}{2\,\epsilon}+\mathcal{O}\left(\epsilon^2\right) \tag{23}$$

$$\boldsymbol{B}\left(\boldsymbol{x},\,\boldsymbol{x}\right) = \frac{\boldsymbol{R}_1-2\,\boldsymbol{R}_0+\boldsymbol{R}_{-1}}{\epsilon^2}+\mathcal{O}\left(\epsilon^3\right) \tag{24}$$

$$\boldsymbol{C}\left(\boldsymbol{x},\,\boldsymbol{x},\,\boldsymbol{x}\right) = \frac{-\boldsymbol{R}_3+8\,\boldsymbol{R}_2-13\,\boldsymbol{R}_1+13\,\boldsymbol{R}_{-1}-8\,\boldsymbol{R}_{-2}+\boldsymbol{R}_{-3}}{8\,\epsilon^3}+\mathcal{O}\left(\epsilon^4\right) \tag{25}$$

where $\boldsymbol{R}_l = \boldsymbol{R}\left(\boldsymbol{x}_0+l\,\epsilon\,\Delta\boldsymbol{x}\right)$. Note that the system Jacobian matrix is in general available in analytic form. To calculate all the terms in Eqs. (20) and (21), a set of identities for the manipulation of terms like $\boldsymbol{B}\left(\boldsymbol{x},\,\boldsymbol{y}\right)$ and $\boldsymbol{C}\left(\boldsymbol{x},\,\boldsymbol{y},\,\boldsymbol{z}\right)$ can be derived. The following two identities

$$\boldsymbol{B}\left(\boldsymbol{x}+\boldsymbol{y},\,\boldsymbol{x}+\boldsymbol{y}\right) = \boldsymbol{B}\left(\boldsymbol{x},\,\boldsymbol{x}\right)+2\,\boldsymbol{B}\left(\boldsymbol{x},\,\boldsymbol{y}\right)+\boldsymbol{B}\left(\boldsymbol{y},\,\boldsymbol{y}\right) \tag{26}$$

$$\boldsymbol{B}\left(\boldsymbol{x}-\boldsymbol{y},\,\boldsymbol{x}-\boldsymbol{y}\right) = \boldsymbol{B}\left(\boldsymbol{x},\,\boldsymbol{x}\right)-2\,\boldsymbol{B}\left(\boldsymbol{x},\,\boldsymbol{y}\right)+\boldsymbol{B}\left(\boldsymbol{y},\,\boldsymbol{y}\right) \tag{27}$$

yield the desired result for the second Jacobian term

$$\boldsymbol{B}\left(\boldsymbol{x},\,\boldsymbol{y}\right) = \frac{1}{4}\Big(\boldsymbol{B}\left(\boldsymbol{x}+\boldsymbol{y},\,\boldsymbol{x}+\boldsymbol{y}\right)-\boldsymbol{B}\left(\boldsymbol{x}-\boldsymbol{y},\,\boldsymbol{x}-\boldsymbol{y}\right)\Big) \tag{28}$$

A similar set of identities is readily derived for $\boldsymbol{C}$ which combined together results in the following general formulation for a third order Jacobian term

$$\boldsymbol{C}\left(\boldsymbol{x},\,\boldsymbol{y},\,\boldsymbol{z}\right) = \frac{1}{6}\Big(\boldsymbol{C}\left(\boldsymbol{x}+\boldsymbol{y}+\boldsymbol{z},\,\boldsymbol{x}+\boldsymbol{y}+\boldsymbol{z},\,\boldsymbol{x}+\boldsymbol{y}+\boldsymbol{z}\right)-\boldsymbol{C}\left(\boldsymbol{x}+\boldsymbol{y},\,\boldsymbol{x}+\boldsymbol{y},\,\boldsymbol{x}+\boldsymbol{y}\right)-\boldsymbol{C}\left(\boldsymbol{x}+\boldsymbol{z},\,\boldsymbol{x}+\boldsymbol{z},\,\boldsymbol{x}+\boldsymbol{z}\right)-\boldsymbol{C}\left(\boldsymbol{y}+\boldsymbol{z},\,\boldsymbol{y}+\boldsymbol{z},\,\boldsymbol{y}+\boldsymbol{z}\right)+\boldsymbol{C}\left(\boldsymbol{x},\,\boldsymbol{x},\,\boldsymbol{x}\right)+\boldsymbol{C}\left(\boldsymbol{y},\,\boldsymbol{y},\,\boldsymbol{y}\right)+\boldsymbol{C}\left(\boldsymbol{z},\,\boldsymbol{z},\,\boldsymbol{z}\right)\Big) \tag{29}$$

[a] Note that $B_i\left(\boldsymbol{x},\,\boldsymbol{y}\right) = B_i\left(\boldsymbol{y},\,\boldsymbol{x}\right)$ and similar properties hold for the third order Jacobian.

Because eigenvalues are complex in general, the formulations in Eqs. (28) and (29) derived for any real vector, $\boldsymbol{x}, \boldsymbol{y}, \boldsymbol{z} \in \mathbb{R}^n$, can be applied to any complex vector when the real and imaginary parts are treated separately. Denoting

$$\boldsymbol{p} \;=\; \boldsymbol{p}_1 \;+\; i\,\boldsymbol{p}_2, \quad \boldsymbol{p} \in \mathbb{C}^n, \quad \boldsymbol{p}_1, \boldsymbol{p}_2 \in \mathbb{R}^n \tag{30}$$

it follows that, for example,

$$\boldsymbol{B}\,(\boldsymbol{p}, \boldsymbol{p}) \;=\; \boldsymbol{B}\,(\boldsymbol{p}_1, \boldsymbol{p}_1) \;-\; \boldsymbol{B}\,(\boldsymbol{p}_2, \boldsymbol{p}_2) \;+\; 2\,i\,\boldsymbol{B}\,(\boldsymbol{p}_1, \boldsymbol{p}_2) \tag{31}$$

and

$$\boldsymbol{C}\,(\boldsymbol{p}, \boldsymbol{p}, \boldsymbol{p}) \;=\; \boldsymbol{C}\,(\boldsymbol{p}_1, \boldsymbol{p}_1, \boldsymbol{p}_1) \;-\; 3\,\boldsymbol{C}\,(\boldsymbol{p}_1, \boldsymbol{p}_2, \boldsymbol{p}_2) \;+\; i\left(3\,\boldsymbol{C}\,(\boldsymbol{p}_1, \boldsymbol{p}_1, \boldsymbol{p}_2) \;-\; \boldsymbol{C}\,(\boldsymbol{p}_2, \boldsymbol{p}_2, \boldsymbol{p}_2)\right) \tag{32}$$

The evaluation of the finite differences suffers from the truncation error for values of the step size ϵ which are too large, and from the rounding error for values which are too small. The latter effect is more significant for the coefficients that include a third Jacobian product. References[11,12] conducted convergence studies and obtained a reliable set of coefficients for the reduced model over a significant range of ϵ.

IV. Optimal Control using Reduced Models

This section describes how linear and nonlinear reduced models were used to design control laws for gust load alleviation. The dynamics of the reduced model is

$$\boldsymbol{z}' \;=\; \boldsymbol{A}\,\boldsymbol{z} \;+\; \boldsymbol{B}_{c1}\,u \;+\; \boldsymbol{B}_{c2}\,u' \;+\; \boldsymbol{B}_{c3}\,u'' \;+\; \boldsymbol{B}_w\,w \tag{33}$$

The matrix $\boldsymbol{A}$ contains the eigenvalues of the coupled system and $\boldsymbol{B}_{c1}, \boldsymbol{B}_{c2}, \boldsymbol{B}_{c3}$ are control derivatives corresponding to rotation, angular velocity and angular acceleration of the control surfaces. The gust terms are given in $\boldsymbol{B}_w$. The system is rewritten introducing the flap rotation and angular velocity into the state vector, with the angular accelaration as a control input.

$$\begin{pmatrix} \boldsymbol{z} \\ u \\ u' \end{pmatrix}' = \begin{pmatrix} \boldsymbol{A} & \boldsymbol{B}_{c1} & \boldsymbol{B}_{c2} \\ \boldsymbol{0} & 0 & 1 \\ \boldsymbol{0} & 0 & 0 \end{pmatrix} \begin{pmatrix} \boldsymbol{z} \\ u \\ u' \end{pmatrix} + \begin{pmatrix} \boldsymbol{B}_{c3} \\ 0 \\ 1 \end{pmatrix} u'' + \begin{pmatrix} \boldsymbol{B}_w \\ 0 \\ 0 \end{pmatrix} w \tag{34}$$

Rewrite the above equation as

$$\boldsymbol{x}' \;=\; \boldsymbol{A}_e\,\boldsymbol{x} \;+\; \boldsymbol{B}_e\,\overline{u} \;+\; \boldsymbol{D}_e\,w \tag{35}$$

where $\overline{u}$ is the flap angular accelaration. The output equation derives from Eq. (16). The complete set of equation become

$$\overline{x'} = \overline{A_e}\,\overline{x} + \overline{D_e}\,w + \overline{B}\,\overline{u} \tag{36}$$

$$\overline{y}_{ctl} = \overline{C_1}\,\overline{x} + \overline{D_{11}}\,w + \overline{D_{12}}\,\overline{u} \tag{37}$$

$$\overline{y}_{meas} = \overline{C_2}\,\overline{x} + \overline{D_{21}}\,w + \overline{D_{22}}\,\overline{u} \tag{38}$$

where C_1, C_2 are the representative eigenvectors of the reduced order model dynamics.

$$\begin{pmatrix} \overline{x}' \\ \overline{y}_{ctl} \\ \overline{y}_{meas} \end{pmatrix} \begin{pmatrix} \overline{A} & \overline{D_e} & \overline{B} \\ \overline{C_1} & \overline{D_{11}} & \overline{D_{12}} \\ \overline{C_2} & \overline{D_{21}} & \overline{D_{22}} \end{pmatrix} \begin{pmatrix} \overline{x} \\ w \\ \overline{u} \end{pmatrix} \tag{39}$$

The output is distinguished by what the controller is aiming to control $\overline{y}_{ctl}$ and what the controller has information about $\overline{y}_{meas}$. The resulting controller has the linear form

$$u(s) = K(s) y_{meas}(s) \tag{40}$$

where $K(s)$ is the H_∞ controller transfer function in the Laplace domain. It is one that aims to minimise the transfer of the disturbance signal from w to y_{ctl} by creating a controller that uses information from y_{meas} to change the input u. This can be written as

$$\frac{sup \int_0^\infty ||\overline{y}_{meas}||^2 dt}{sup \int_0^\infty ||w(t)||^2 dt} \leq \gamma \tag{41}$$

where γ represents the ratio of the maximum output energy to the maximum input energy.

The problem is expanded to include a weight on inputs (K_c) which carries over to an additional element on controlled output and a weight on measurement noise (K_d) which carries over to an additional element on measured output. The control will be done in the same way when using a nonlinear reduced model. The dynamics of the nonlinear reduced model is the same as for the linear model with the addition of vector where nonlinearities are contained. The H_∞ control is derived for the linearized model and is applied directly to the nonlinear model by utilizing the reduced matrices from the nonlinear model order reduction.

V. Aerofoil Results

The test problem considered is for an aerofoil section at zero incidence. The parameters for the structural model are given in Table 1. The testcase corresponds to the "heavy case" described in Ref.[24] The traces of the pitching and plunging modes for increasing reduced velocity are shown in Fig. 2. The instabilty occurs for $U_L^* = 4.6137$. The code has been validated against other independent investigations, and more details on this can be found in Ref.[13]

Parameter	Value
$\bar{\omega}$	0.343
μ	100.0
a_h	-0.2
x_α	0.2
r_α	0.539

Table 1. Reference values of the pitch-plunge aerofoil model for the "heavy case"

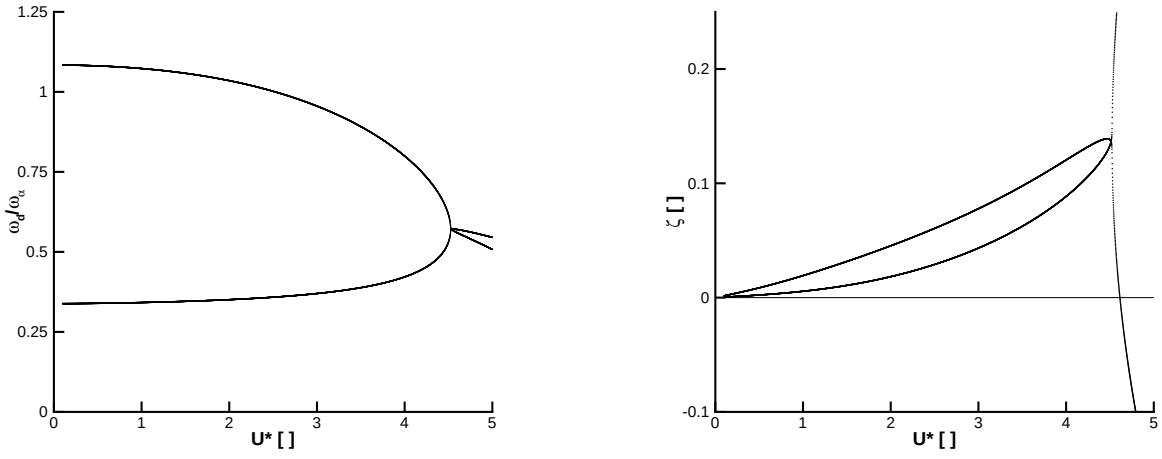

(a) Frequency ratio, ω_d/ω_α

(b) Damping ratio, ξ

Figure 1. Eigenvalue tracing of aerofoil model

To generate the reduced model in Eq. (16), the eigenvectors of the coupled system are required. This is done here using standard routines readily available for the solution of the eigenvalue problem. In the case of

a system of millions of unknowns, as for the test cases documented in a companion paper,[25] the eigenvalue problem is solved with an alternative method.

For the aerofoil results with linear structure, the eigenvector basis was calculated only once at a reduced velocity of 4.6, which corresponds to 99.7% of the flutter speed.

V.A. Evaluation of the Reduced Model

The reduced model was first tested for a problem without gust encounter. The initial condition driving both reduced and full model responses is a perturbation in plunge velocity, $\xi' = 0.01$. The reduced velocity is 99.7% of the flutter speed. The agreement between the reduced and full models shown in Fig. 2 is satisfactory. The decay of oscillations is slow because the system is very close to the instability point. This is an interesting condtion because a gust encounter of sufficient intensity could trigger an instability in the system response.

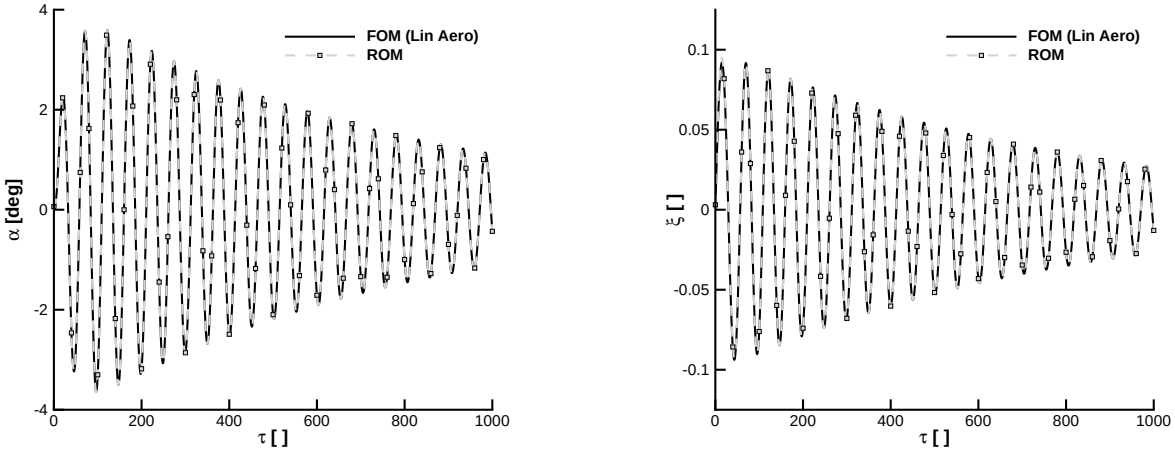

(a) Pitch, α (b) Plunge, ξ

Figure 2. Free response of aerofoil model to $\xi' = 0.01$ at $U^* = 4.6$

The gust term was then added to the reduced model, and the comparison for a "1 minus cosine" gust of intensity 5% of the freestream speed and length 25 chords was made. The time response from the reduced and full order models is shown in Fig. 3, and shows that the reduced model is accurate to use it for worst case gust search, which is presented in the next section.

V.B. Worst-Case Gust Search

The reduced model is used to perform a worst case gust search for the "1 minus cosine" family. The gust intensity is 5% of the freestream speed at $U^* = 4.6$, and the search is made for gust lengths up to 100 aerofoil semi-chords. The parameter space is divided into 1000 design sites, and Kriging interpolation is used to drive the search and obtain the maximum and minimum responses in Fig. 4. The worst case gust was found to be for $H_g = 41$ corresponding to a frequency close to the coupled system eigenvalue.

V.C. Control Design for Load Alleviation

Having established and tested the reduced model for several conditions, it is now possible to exploit it for gust load alleviation. The method documented here can be extended in a straighforward manner to systems of larger dimension, for example given by CFD. The strength of the approach is to allow control design to be done on a state space system of small size which is independent of the underlying physical model.

The control design for the worst case gust is done using the standard H^∞ technique. The control effector is the trailing-edge flap and the pitch degree of freedom is measured for feedback. The open and closed loop responses are compared in Fig. 5, and a significant alleviation in both degrees of freedom is achieved with a reasonable control input.

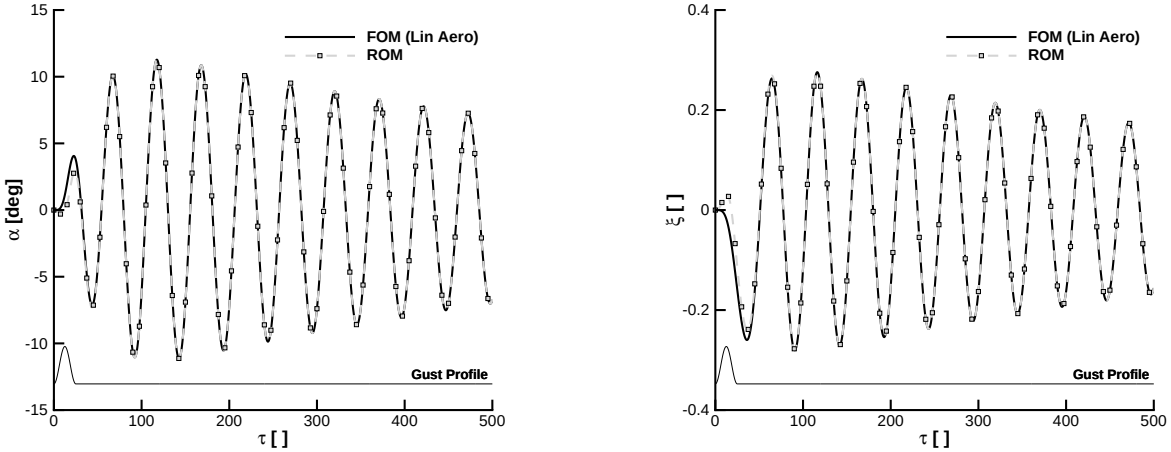

(a) Pitch, α (b) Plunge, ξ

Figure 3. Response to a "1 minus cosine" gust of intensity 5% of the freestream speed and length 25 chords at $U^* = 4.6$

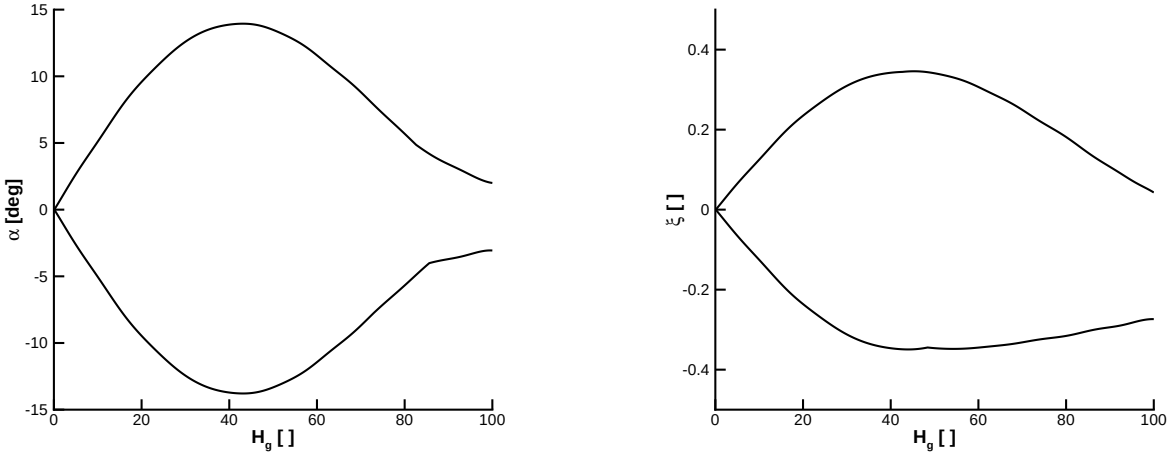

(a) Pitch, α (b) Plunge, ξ

Figure 4. Worst-case gust search at $U^* = 4.6$ for "1 minus cosine" gust of constant intensity $w_g = 0.05$

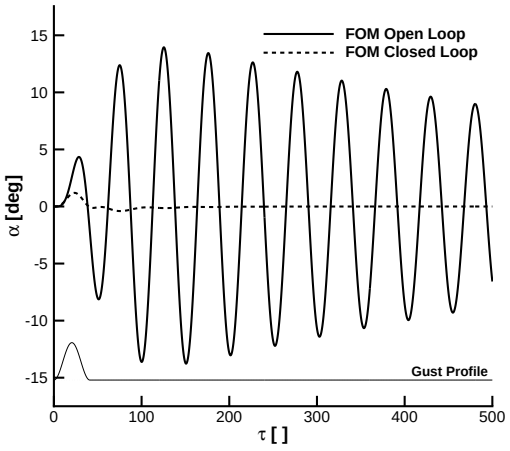

(a) Pitch, α

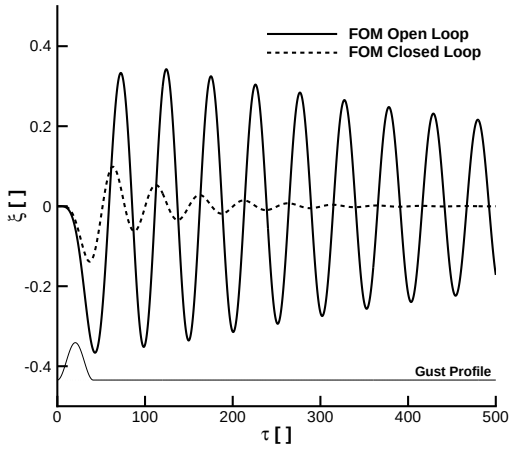

(b) Plunge, ξ

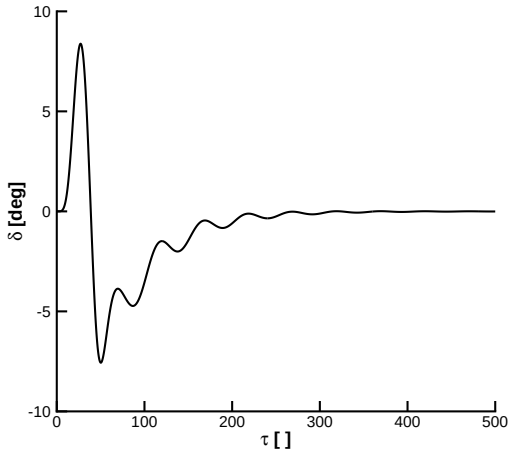

(c) Flap Rotation, δ

Figure 5. Open-loop and closed-loop responses for the worst-case gust

In the case that the full order model exhibits a nonlinear behaviour in the gust response, quadratic and cubic terms are included in the reduced model in a straight-forward fashion. Consider, for example, the full model responses in Fig. 6. The nonlinearity in the full order model was obtained by adding a cubic spring constant in both pitch and plunge degrees of freedom. The effect of structural nonlinearity is evident. Nonlinear terms were then generated for the reduced model, and the predictions shown in figure are in good agreement with the nonlinear full model.

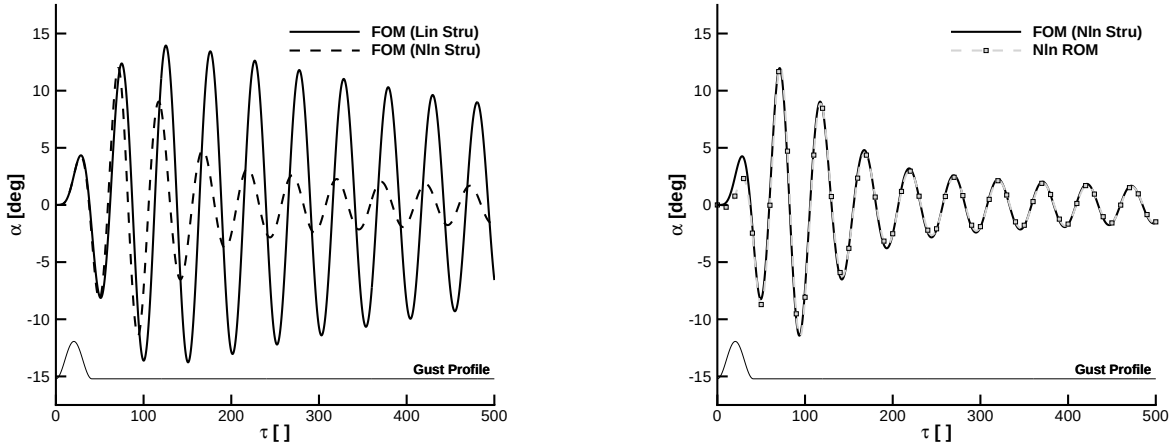

(a) Linear/nonlinear full order models

(b) Nonlinear full and reduced order models

Figure 6. Response to a "1 minus cosine" gust of intensity 5% of the freestream speed and length 25 chords at $U^* = 4.6$

The ability to retain relevant nonlinearities in the reduced model is exploited for gust loads alleviation. The control design was performed as in the linear case, with the exception that the reduced model now includes the nonlinear vector in Eq. (21). Comparing the time responses in Fig. 7 indicates a good alleviation in the pitch motion. The control deflection required is similar to the linear case, as the nonlinearity used here reduces the system response.

The approach to control design based on a nonlinear reduced model is general, and could be applied to a variety of nonlinear problems. An interesting application is gust loads alleviation from a reduced model derived from CFD. Future work will focus on this. The next section deals with a full order model where nonlinearities in the structure are modelled using the geometrically-nonlinear beam equations.

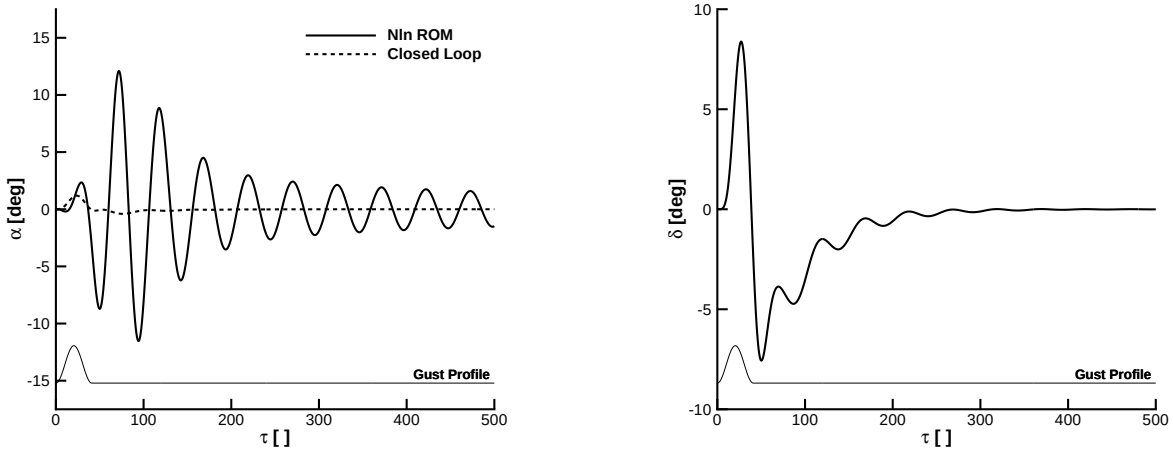

(a) Pitch, α

(b) Flap Rotation, δ

Figure 7. Open-loop and closed-loop responses for the aerofoil with structural nonlinearity

VI. Unmanned Aerial Vehicle Results

The test case used in this paper is based on a model produced by Peter Hopgood of DSTL for research purposes, and is shown in Fig. 8. The structural model consists of high aspect ratio wings and a V-tail, each having a single pair of trailing-edge control surfaces. The structural mass of the aircraft is 4732.5 Kg, with the centre of gravity at 6.382 m from the nose. Non-structural masses are used to model fuel loads in the wing box. The front and rear spars are located at 15 and 77% of the local chord of the wing, and at 15 and 80% of the local chord of the V-tail.

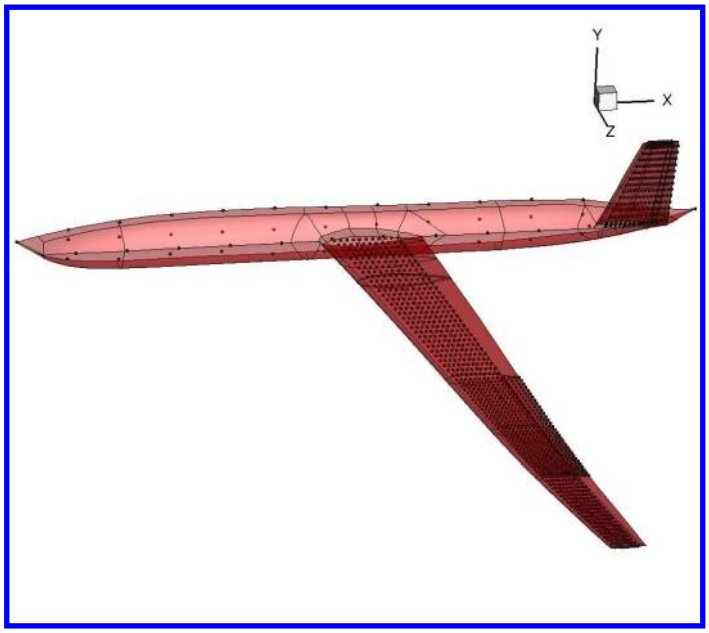

Figure 8. Geometry of a UAV configuration

Additional geometric characteristics are shown in Table 2. For this paper, a half model was used which is clamped at the node connecting the main wing with the fuselage.

Parameter	Wing [m]	Tail [m]
Span	17.71	3.23
Root chord	1.66	1.393
Tip chord	0.733	0.678

Table 2. Geometrical characteristics of the UAV test case

VI.A. Model Tuning

A beam model was created starting from a detailed finite element model. The beam structural model of the wing has 20 elements while for the fuselage and the tail 4 and 3 elements were used, respectively. The structural model has varying stiffness and mass matrices along the wing span and those values were used to tune the modal frequencies and shapes against the original NASTRAN model. The natural frequencies of the lowest mode shapes from the original model and the beam model are summarised in Table 3. The third bending mode mapped to the aerodynamic surface is shown in Fig. 9. As expected, the agreement is good at low frequencies and deteriorates at higher frequencies. The following investigations are based on this beam model considered sufficiently accurate for the purpose of this work, which is on the exploitation of reduced models for control design.

Mode	Modeshape	Original Model [Hz]	Beam Model [Hz]
1	Wing First Bending	3.56	3.48
2	Wing Second Bending	7.75	6.99
3	Wing First In-plane Bending	11.50	7.79
4	Wing First Torsion	14.9	12.2
5	Wing Third Bending	15.7	17.6
6	Wing Fourth Bending	24.6	27.6
7	Tail First Bending	45.4	34.8
8	Tail First Torsion	94.1	87.9

Table 3. Modeshapes of the UAV test case from the original NASTRAN model and the beam model

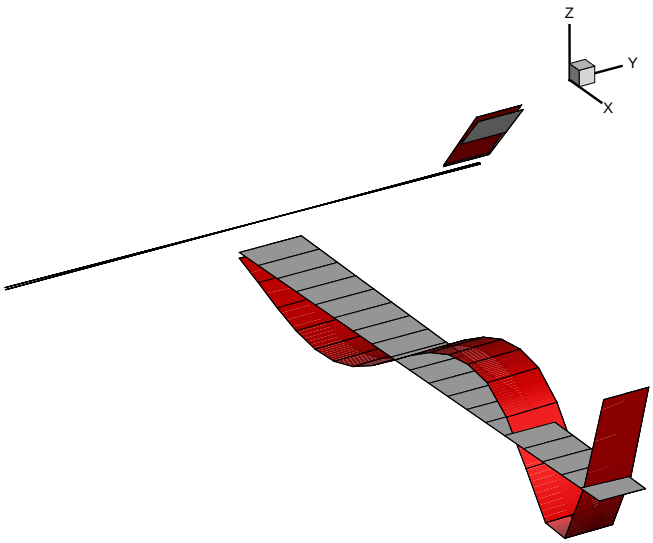

Figure 9. Third bending mode of the UAV test case mapped to the aerodynamic surface

VI.B. Evaluation of the Reduced Model

The generation of the reduced model was done at Mach number 0.08 and altitude 20,000 m for a freestream angle of attack of 5.0 deg. At this condition, the wing deforms of about 0.12 m. To form the eigenvector basis for model projection, an eigenvalue problem is solved for the coupled system which contains 540 degrees of freedom. There are several options to select the basis for the reduced model. Low frequency normal modes of the structure influenced by the coupling with the aerodynamics are first included in the basis. In the case that the coupling of the structure with the aerodynamics is important, as in a gust response analysis, additional modes are added. These modes introduce information about the gust encounter. The basis created in this way is complete, in the sense that it will prove adequate to represent the dynamics of the full order model.

The convergence of reduced model predictions to a "1 minus cosine" gust for increasing number of eigenvectors is shown in Fig. 10. Few aerodynamic modes corresponding to the gust terms in the Küssner formulation are sufficient to obtain a response which is virtually identical to the full model response. In this case, a reduction from 540 degrees of freedom for the full model to 16 was achieved.

Tests were made for the gust response to a continuous atmospheric turbulence. The same reduced model was used. The gust time history was generated using the Von Kármán spectrum. Considering the time responses in Fig. 11, a good agreement of the reduced order model with the full model for the entire simulation is observed.

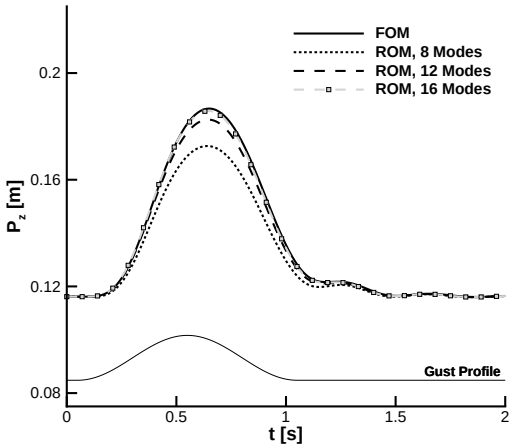

Figure 10. Vertical wing tip displacement to a "1 minus cosine" gust of intensity 6% of the freestream speed for increasing number of modes

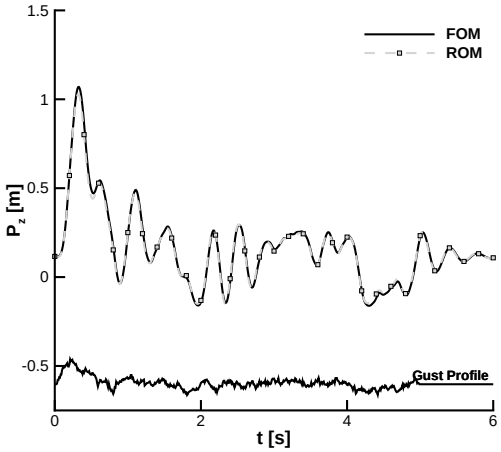

Figure 11. Vertical wing tip displacement to a continuous gust

The assessment of the reduced order model for various types of gust disturbance confirmed the adequacy of the reduced model, and it is now used to develop a control strategy for gust load alleviation.

VI.C. Worst-Case Gust Search

The reduced model was used to identify the worst-case gust from the "1 minus cosine" family. In this case, the gust intensity, w_g, was related to the gust length by the relation $w_g \propto H^{1/3}$. The same approach detailed for the aerofoil test case to drive the search and interpolate calculations of the reduced model was used here. The worst-case gust was found to be for 50 semi-chords, which is a typical value recommended for gust response analysis. Note that it would be possible to extend the search to more gust parameters or flight conditions while exploiting the same reduced model.

VI.D. Control Design for Load Alleviation

The design of a controller for load alleviation was done on the reduced model using the worst-case gust. The good performance of the controller to suppress the vibrations induced by the worst-case gust is not unexpected, as the controller was designed specifically for that condition. This was also noted for the aerofoil test case. The question addressed in this section is whether a good alleviation can be achieved when considering a different gust type, but using the same controller. The responses shown in Fig. 12 are for a continuous gust model based on Von Kármán spectrum. The vibrations of the closed loop system are significantly reduced when compared to the open loop response.

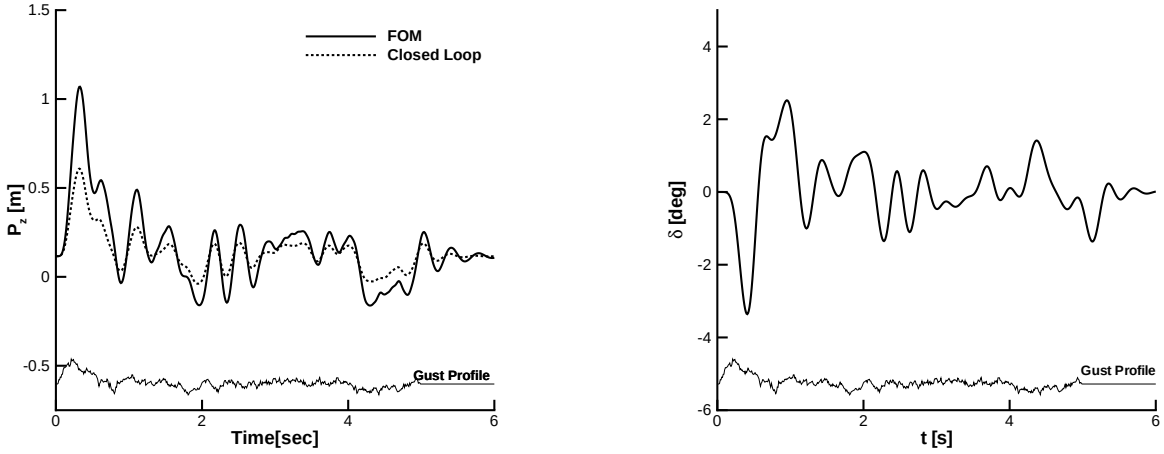

(a) Wing tip vertical displacement, P_z

(b) Flap Rotation, δ

Figure 12. Open-loop and closed-loop responses for a continuous gust

The efficiency of the optimal control approach using the reduced models for gust load alleviation can be demonstrated in a case with noticeable differences between the linear and nonlinear full order models. The freestream angle of attack is 10 deg, the altitude is 9,500 ft and the mach number 0.1. The response of the full and reduced models is shown in Fig. 13. The closed loop responses are shown in Fig. 14.

VII. Conclusions

A systematic approach to model reduction for control applications has been considered. The approach is independent of the full order model and can be applied to any system formulated in a standard state space form. The generation of the reduced order model is done solving an eigenvalue problem of the coupled system. The emphasis of this work was on the exploitation of these systems of small size for control studies. Two test cases were considered, subject to discrete and continuous gust models. The first test case was a two degree-of-freedom aerofoil section and the second test case was a unmanned aerial vehicle model. Control design has been shown starting from the full order models, and tested for various families of atmospheric gusts. In

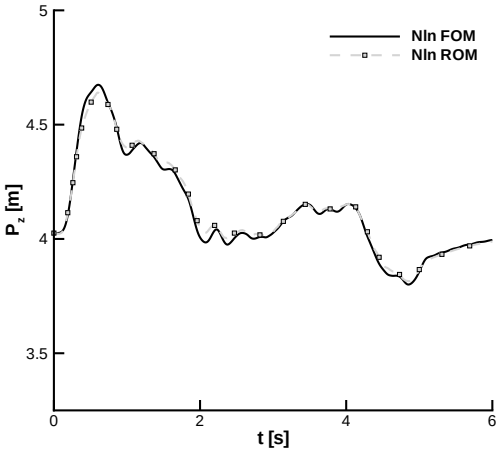

(a) Wing tip vertical displacement P_z

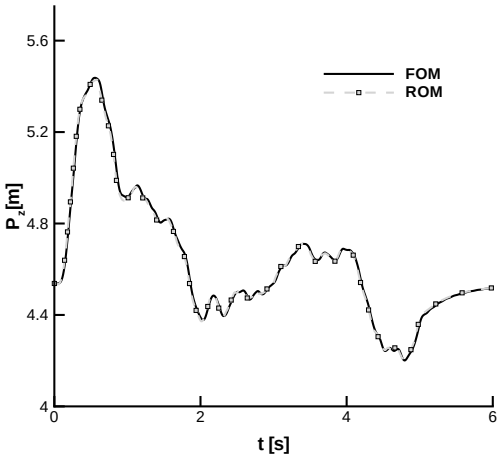

(b) Wing tip vertical displacement

Figure 13. Responses from linear and nonlinear full/reduced order models

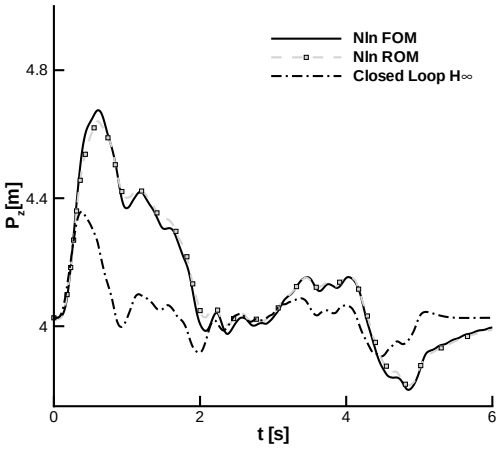

(a) Wing tip vertical displacement P_z

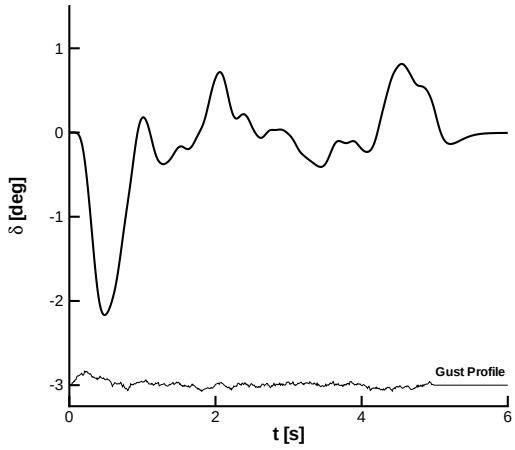

(b) Flap Rotation, δ

Figure 14. Open-loop and closed-loop responses for a continuous gust

the case that the full order model is highly nonlinear, nonlinear terms were included in a straight-forward fashion into the reduced model.

Future work involves the application of the method to free flying aircraft configurations.

VIII. Acknowledgments

This work was supported by the U.K. Engineering and Physical Sciences Research Council (EPSRC). Thanks to R. N. Palacios of Imperial College, London, for providing the nonlinear beam code.

References

[1]Noll, T. E., Brown, J. M., Perez-Davis, M. E., Ishmael, S. D., Tiffany, G. C., and Gaier, M., "Investigation of the Helios Prototype Aircraft Mishap," NASA Tech. Rep., January, 2004.

[2]Palacios, R., Murua, J., and Cook, R., "Structural and Aerodynamic Models in Nonlinear Flight Dynamics of Very Flexible Aircraft," *AIAA Journal*, Vol. 48, No. 11, 2010, pp. 2648–2659, doi: 10.2514/1.52446.

[3]Silva, W., "Identification of Nonlinear Aeroelastic Systems based on the Volterra Theory: Progress and Opportunities," *Nonlinear Dynamics*, Vol. 39, No. 1–2, 2005, pp. 25–62, doi: 10.1007/s11071-005-1907-z.

[4]Da Ronch, A., Vallespin, D., Ghoreyshi, M., and Badcock, K. J., "Evaluation of Dynamic Derivatives Using Computational Fluid Dynamics," *AIAA Journal*, Vol. 50, No. 2, 2012, pp. 470–484, doi: 10.2514/1.J051304.

[5]Da Ronch, A., McCracken, A., Badcock, K. J., Ghoreyshi, M., and Cummings, R. M., "Modeling of Unsteady Aerodynamic Loads," *Atmospheric Flight Mechanics Conference*, AIAA–2011–2376, Portland, Oregon, 2011.

[6]Da Ronch, A., Ghoreyshi, M., and Badcock, K. J., "On the Generation of Flight Dynamics Aerodynamic Tables by Computational Fluid Dynamics," *Progress in Aerospace Sciences*, Vol. 47, No. 8, 2011, pp. 597–620, doi: 10.1016/j.paerosci.2011.09.001.

[7]Vallespin, D., Badcock, K. J., Da Ronch, A., White, M. D., Perfect, P., and Ghoreyshi, M., "Computational Fluid Dynamics Framework for Aerodynamic Model Assessment," *Progress in Aerospace Sciences*, Vol. 52, 2012, pp. 2–18, doi: 10.1016/j.paerosci.2011.12.004.

[8]Lucia, D. J., Beran, P. S., and Silva, W. A., "Reduced-Order Modeling: New Approaches for Computational Physics," *Progress in Aerospace Sciences*, Vol. 40, No. 1–2, 2004, pp. 51–117, doi: 10.1016/j.paerosci.2003.12.001.

[9]Da Ronch, A., McCracken, A., Badcock, K. J., Widhalm, M., and Campobasso, M. S., "Linear Frequency Domain and Harmonic Balance Predictions of Dynamic Derivatives," *Journal of Aircraft*, Accepted for Publication 2012 [see also AIAA Paper 2010–4699].

[10]Mialon, B., Khrabrov, A., Khelil, S. B., Huebner, A., Da Ronch, A., Badcock, K. J., Cavagna, L., Eliasson, P., Zhang, M., Ricci, S., Jouhaud, J.-C., Rogé, G., Hitzel, S., and Lahuta, M., "Validation of Numerical Prediction of Dynamic Derivatives: The DLR-F12 and the Transcruiser Test Cases," *Progress in Aerospace Sciences*, Vol. 47, No. 8, 2011, pp. 674–694, doi: 10.1016/j.paerosci.2011.08.010.

[11]Woodgate, M. A. and Badcock, K. J., "Fast Prediction of Transonic Aeroelastic Stability and Limit Cycles," *AIAA Journal*, Vol. 45, No. 6, 2007, pp. 1370–1381, doi: 10.2514/1.25604.

[12]Badcock, K. J., Woodgate, M. A., Allan, M. R., and Beran, P. S., "Wing-Rock Limit Cycle Oscillation Prediction based on Computational Fluid Dynamics," *Journal of Aircraft*, Vol. 45, No. 3, 2008, pp. 954–961, doi: 10.2514/1.32812.

[13]Da Ronch, A., Badcock, K. J., Wang, Y., Wynn, A., and Palacios, R. N., "Nonlinear Model Reduction for Flexible Aircraft Control Design," *AIAA Atmospheric Flight Mechanics Conference*, AIAA Paper 2012–4404, 2012.

[14]Li, D., Guo, S., and Xiang, J., "Aeroelastic Dynamic Response and Control of an Airfoil Section with Control Surface Nonlinearities," *Journal of Sound and Vibration*, Vol. 329, 2010, pp. 4756–4771, doi: 10.1016/j.jsv.2010.06.006.

[15]Strganac, T. W., Ko, J., Thompson, D. E., and Kurdila, A. J., "Identification and Control of Limit Cycle Oscillations in Aeroelastic Systems," *Journal of Guidance, Control, and Dynamics*, Vol. 23, No. 6, 2000, pp. 1127–1133.

[16]Dillsaver, M. J., Cesnik, C. E. S., and Kolmanovsky, I. V., "Gust Load Alleviation Control for Very Flexible Aircraft," *AIAA Atmospheric Flight Mechanics Conference*, AIAA Paper 2011–6368, 2011.

[17]Gibson, T. E., Annaswamy, A. M., and Lavretsky, E., "Modeling for Control of Very Flexible Aircraft," *AIAA Guidance, Navigation, and Control Conference*, AIAA Paper 2011–6202, 2011.

[18]Lee, B. H. K., Gong, L., and Wong, Y. S., "Analysis and Computation of Nonlinear Dynamic Response of a Two-Degree-of-Freedom System and Its Application in Aeroelasticity," *Journal of Fluids and Structures*, Vol. 11, No. 3, 1997, pp. 225–246, doi: 10.1006/jfls.1996.0075.

[19]Campbell, C. W., "Monte Carlo Turbulence Simulation Using Rational Approximations to Von Kármán Spectra," *AIAA Journal*, Vol. 24, No. 1, 1986, pp. 62–66, doi: 10.2514/3.9223.

[20]Meirovitch, L., *Dynamics and Control of Structures*, Wiley, New York, 1989, pp. 93–98.

[21]Pettit, C. L. and Beran, P. S., "Effects of parametric uncertainty on airfoil limit cycle oscillation," *Journal of Aircraft*, Vol. 40, No. 5, 2003, pp. 1004–1006.

[22]Hodges, D. H., "A mixed variational formulation based on exact intrinsic equations for dynamics of moving beams," *International Journal of Solids and Structures*, Vol. 26, No. 11, 1990, pp. 1253–1273, doi: 10.1016/0020-7683(90)90060-9.

[23]Badcock, K. J. and Woodgate, M. A., "Bifurcation Prediction of Large-Order Aeroelastic Models," *AIAA Journal*, Vol. 48, No. 6, 2010, pp. 1037–1046, doi: 10.2514/1.40961.

[24]Badcock, K. J., Woodgate, M., and Richards, B. E., "Hopf Bifurcation Calculations for a Symmetric Airfoil in Transonic Flow," *AIAA Journal*, Vol. 42, No. 5, 2004, pp. 883–892, doi: 10.2514/1.9584.

[25]Da Ronch, A., Tantaroudas, N. D., Timme, S., and Badcock, K. J., "Model Reduction for Linear and Nonlinear Gust Loads Analysis," *54th AIAA/ASME/ASCE/AHS/ASC Structures, Structural Dynamics and Materials Conference*, AIAA Paper 2013, Boston, Massachusetts, 2013.